ACS APPLIED MATERIALS & INTERFACES

Research Article

www.acsami.org

# Aluminum Nitride Hydrolysis Enabled by Hydroxyl-Mediated Surface Proton Hopping

Christopher J. Bartel,[†] Christopher L. Muhich,[†,§] Alan W. Weimer,[*,†] and Charles B. Musgrave[*,†,‡]

[†]Department of Chemical and Biological Engineering and [‡]Department of Chemistry and Biochemistry, University of Colorado, Boulder, Colorado 80309, United States

[§]Department of Mechanical and Process Engineering, ETH Zurich, 8092 Zurich, Switzerland

Supporting Information

**ABSTRACT:** Aluminum nitride (AlN) is used extensively in the semiconductor industry as a high-thermal-conductivity insulator, but its manufacture is encumbered by a tendency to degrade in the presence of water. The propensity for AlN to hydrolyze has led to its consideration as a redox material for solar thermochemical ammonia ($NH_3$) synthesis applications where AlN would be intentionally hydrolyzed to produce $NH_3$ and aluminum oxide ($Al_2O_3$), which could be subsequently reduced in nitrogen ($N_2$) to reform AlN and reinitiate the $NH_3$ synthesis cycle. No quantitative, atomistic mechanism by which AlN, and more generally, metal nitrides react with water to become oxidized and generate $NH_3$ yet exists. In this work, we used density-functional theory (DFT) to examine the reaction mechanisms of the initial stages of AlN hydrolysis, which include: water adsorption, hydroxyl-mediated proton diffusion to form $NH_3$, and $NH_3$ desorption. We found activation barriers ($E_a$) for hydrolysis of 330 and 359 kJ/mol for the cases of minimal adsorbed water and additional adsorbed water, respectively, corroborating the high observed temperatures for the onset of steam AlN hydrolysis. We predict AlN hydrolysis to be kinetically limited by the dissociation of strong Al−N bonds required to accumulate protons on surface N atoms to form $NH_3$. The hydrolysis mechanism we elucidate is enabled by the diffusion of protons across the AlN surface by a hydroxyl-mediated Grotthuss mechanism. A comparison between intrinsic ($E_a$ = 331 kJ/mol) and mediated proton diffusion ($E_a$ = 89 kJ/mol) shows that hydroxyl-mediated proton diffusion is the predominant mechanism in AlN hydrolysis. The large activation barrier for $NH_3$ generation from AlN ($E_a$ = 330 or 359 kJ/mol, depending on water coverage) suggests that in the design of materials for solar thermochemical ammonia synthesis, emphasis should be placed on metal nitrides with less covalent metal−nitrogen bonds and, thus, more-facile $NH_3$ liberation.

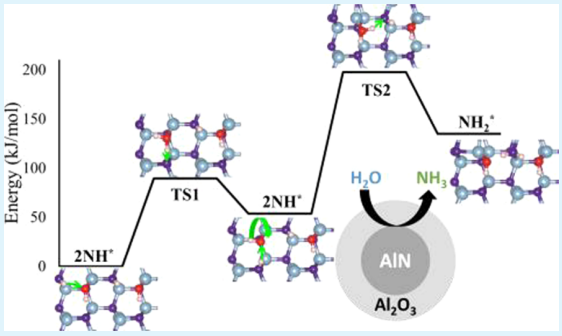


**KEYWORDS:** *metal nitride, hydrolysis, corrosion, density functional theory, proton hopping, thermochemical redox, ammonia synthesis*

## 1. INTRODUCTION

Aluminum nitride (AlN) is a large, direct-band-gap semiconducting material with a unique array of properties including high thermal conductivity (319 $Wm^{-1}K^{-1}$, theoretical at room temperature),[1] low electrical conductivity (resistivity >$10^{13}$ Ω cm),[2] high mechanical strength (>400 MPa),[3] and a thermal expansion coefficient (4.3 × $10^{-6}$ $K^{-1}$ at room temperature)[2] near that of silicon. This remarkable combination of properties makes AlN highly valuable as a packaging material for integrated circuits and multichip modules. However, the propensity for AlN to hydrolyze and produce ammonia ($NH_3$) precludes the use of water during its processing, mandating the use of organic solvents, such as isopropanol, which increases the cost and complexity of manufacturing AlN substrates.[4] Despite these challenges, dense, polycrystalline AlN has been implemented as a substrate in high-power microelectronics for over three decades.[5] Currently, polycrystalline AlN is primarily produced commercially by two processes: carbothermal nitridation, which involves nitridation of carbon and alumina ($Al_2O_3$) powders,[6] and direct nitridation,[7] which involves the nitridation of atomized aluminum.

With the continued advances of nanotechnology and device scaling, the electronics industry is faced with the progressively more difficult challenge of thermal management of increasingly dense electronics and integrated circuits. This is even a major issue for power electronics with their low device densities. For instance, thermal management is especially critical in the case of light-emitting diodes (LEDs) where, in general, LED lumen efficiency drops by 0.3−0.5% for every 1 °C increase in operating temperature,[8] and consequently, heat dissipation is an important factor in determining LED performance. Therefore, efforts to develop more efficient heat-dissipation technologies in LED substrates have led to a transition away

Received: April 13, 2016
Revised: June 7, 2016
Accepted: June 24, 2016
Published: June 24, 2016





DOI: 10.1021/acsami.6b04375
ACS Appl. Mater. Interfaces 2016, 8, 18550−18559

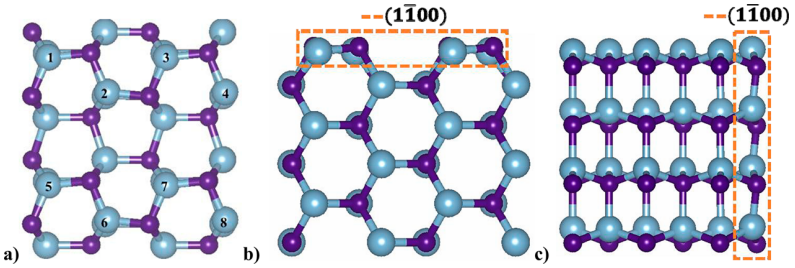


**Figure 1.** (a) Supercell model (2 × 2) of the (1$\bar{1}$ 00) surface (top-down view). (b) Supercell with six layers (side view). (c) Supercell with six layers (side view). The smaller purple spheres represent nitrogen atoms, and the larger blue spheres represent aluminum atoms. Surface Al atoms are labeled 1 through 8 for reference.

from $Al_2O_3$, with a fully dense thermal conductivity of 20−35 $Wm^{-1}K^{-1}$ at room temperature,[9] to AlN, with a polycrystalline thermal conductivity exceeding 200 $Wm^{-1}K^{-1}$.[10−12] However, to achieve these high thermal conductivities, AlN must be processed under strict conditions to avoid oxidation via hydrolysis because oxygen impurities in AlN have been identified as the primary cause of reduced thermal conductivity of dense AlN.[13−15] In fact, reducing the intragranular oxygen content by 50% has been shown to increase the thermal conductivity of dense parts by as much as 41%.[16] This motivated a number of studies that investigated functionalization of the AlN surface to prevent hydrolysis.[17−21] Although some success has been achieved in delaying the onset of hydrolysis in aqueous environments, these approaches involve the use of surface treatments that themselves can decrease the thermal conductivity of AlN.

AlN has also drawn interest as a metal-nitride redox material for $NH_3$ production from steam as a renewable alternative to the energy- and fossil-fuel-intensive Haber-Bosch process with significantly lower environmental impact. Numerous research efforts have sought an atmospheric pressure alternative to the Haber-Bosch process,[22] which operates at extremely high pressure (up to 30 MPa)[23] and consumes approximately 2% of the world's energy production in the form of fossil fuels to both produce the $H_2$ that eventually becomes incorporated into $NH_3$ and drive the technologically challenging conversion of $H_2$ and $N_2$ to $NH_3$.[24] In recent years, a strategy analogous to redox cycling for solar thermochemical water splitting[25] has emerged for the production of $NH_3$ using solar energy to drive a thermochemical redox cycle where a metal oxide is reduced with hydrogen, carbon monoxide, or solid carbon in the presence of nitrogen to produce a metal nitride that is subsequently hydrolyzed by steam to reform the metal oxide and produce $NH_3$.[26−32] For a cycle using AlN as the metal-nitride redox material,[26] the reduction step is shown as reaction 1, and the desired hydrolysis of AlN step is shown as reaction 2:

$$Al_2O_3 + N_2 + 3C \rightleftarrows 2AlN + 3CO \quad (1)$$

$$2AlN + 3H_2O \rightleftarrows 2NH_3 + Al_2O_3 \quad (2)$$

The viability of this alternative route to $NH_3$ production is dependent upon a robust metal-nitride redox material with favorable thermodynamics and kinetics for the reduction and oxidation reactions, i.e., reactions 1 and 2. To understand how to design redox materials to accommodate both reactions favorably, a fundamental understanding of the detailed, active reaction mechanisms is paramount.

Only a few studies of the kinetics of metal-nitride hydrolysis have been reported,[26,32−36] and a quantitative description of the hydrolysis mechanism and bonding in metal nitrides is lacking.[29] Previous experimental work has described hydrolysis subsequent to the initial oxidation of AlN to form an oxidized film using a shrinking core model, which has been utilized to describe the kinetics of hydrolysis and to elucidate the associated kinetic parameters for this reaction.[26,29] However, there has been some disagreement in the literature as to the identity of the rate-determining step for AlN hydrolysis. It has been suggested that AlN hydrolysis is limited by either solid-state diffusion[29] or by the initial surface reactions required to liberate N from the AlN lattice.[26] The lack of a detailed and quantitative mechanistic description increases the challenge of engineering metal nitrides to either increase the rate of hydrolysis for thermochemical $NH_3$ generation or decrease this rate to render particles hydrolysis-resistant. In this work, we report a detailed mechanism of AlN hydrolysis predicted using density functional theory (DFT), which identifies the surface reactions that control the rate of AlN hydrolysis and their associated activation barriers. We found that hydroxyl-mediated surface proton diffusion enables the accumulation of protons to form $NH_3$. Although the diffusion of protons on surfaces by either intrinsic or mediated processes is a key step in a number of important processes, including catalytic hydrogenation[37] and dehydrogenation,[38] hydrogen storage,[39] and conductivity in fuel cells,[40] detailed investigations of surface proton diffusion have been primarily limited to titania[41−43] and, more recently, iron oxide.[44] In this work, we use DFT to investigate the mechanism of AlN hydrolysis and the roles of intrinsic and hydroxyl-mediated surface proton diffusion in AlN hydrolysis.

## 2. RESULTS AND DISCUSSION

We conducted periodic plane wave DFT calculations using the PBE functional to describe reactions of $H_2O$ with the (1$\bar{1}$ 00) AlN surface, shown in Figure 1. We modeled the AlN (1$\bar{1}$ 00) surface using a 96 atom slab to describe the reaction mechanism of the initial hydrolysis of AlN, which generates $NH_3$ and introduces oxygen into the AlN lattice. In the (1$\bar{1}$ 00) AlN surface, subsurface (bulk) Al atoms form four bonds with N. Likewise, subsurface N atoms form four bonds with Al. These bonds are of approximately 75% covalent and 25% dative character because the lone pair of nitrogen forms a dative bond with the empty $sp^3$ orbital of Al. Surface Al atoms are bonded to two surface N atoms and one subsurface N. Likewise, surface N atoms are bonded to two surface Al atoms and one subsurface Al. These bonds are nominally covalent but possess some ionic character due to the electronegativity difference between N and Al. Surface N atoms possess a lone pair, and surface Al atoms possess an empty orbital that create surface Lewis base and acid sites, respectively.



DOI: 10.1021/acsami.6b04375
ACS Appl. Mater. Interfaces 2016, 8, 18550−18559

We found that $H_2O$ reacts with AlN to hydrolyze the surface through four primary steps: (1) water adsorption, (2) proton migration to form $NH_2$* and $NH_3$*, (3) N surface vacancy formation and immediate filling by O*, and (4) $NH_3$* desorption. Throughout the text, "*" denotes a surface species. Details of the calculations can be found in the Methods section.

**2.1. Water Adsorption and Dissociation.** The initial hydrolysis of the bare AlN surface (Figure 1) commences with molecular $H_2O$ adsorption followed by dissociation. We determined the preferred $H_2O$ adsorption geometry by relaxing six unique initial configurations of adsorbed $H_2O$. These initial configurations all relaxed to the molecularly adsorbed state $H_2O$* shown in Figure 2a with an exothermic adsorption

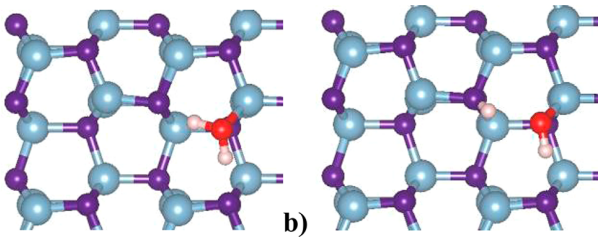


**Figure 2.** (a) Molecular adsorption of $H_2O$ to form $H_2O$*. (b) Dissociation of $H_2O$* to form NH* and strengthen the Al−OH* bond. The purple spheres represent N atoms, light blue spheres represent Al atoms, red spheres represent O atoms, and white spheres represent H atoms.

energy of $E_{ads}$ = −162 kJ/mol. In this state, $H_2O$* acts as a Lewis base where an oxygen lone pair donates into the empty $sp^3$ orbital of the surface Al atom, which acts as a Lewis acid, to form an Al−O dative bond. However, the relaxation mixes the bond character of the Al atom's Al−O bond and its three Al−N bonds to produce bonds of mixed dative−covalent character (Figure 2a). The two neighboring N surface atoms hydrogen bond through their lone pairs with each H atom of $H_2O$* to further stabilize the molecularly adsorbed state.

Once adsorbed on the surface, $H_2O$* readily dissociates (Figure 2b) with a reaction energy and activation barrier of −31 and 3 kJ/mol, respectively. This results in an adsorption energy for the $H_2O$ dissociated state (NH* and Al−OH*) of −193 kJ/mol. The exothermicity of adsorption in both the molecularly and dissociatively adsorbed states is primarily attributed to the formation of Al−OH* and N−H* bonds of mixed dative−covalent character, with further stabilization provided by the two H-bonds formed in both states.

At least two water molecules must dissociate to provide the three hydrogen atoms required for $NH_3$* formation. Therefore, we considered the adsorption of a second $H_2O$ molecule at each of the remaining bare Al sites of the surface supercell in the configuration depicted in Figure 2b. The most favorable dissociative adsorption configuration for the second adsorbing $H_2O$ is shown in Figure 3a. This configuration for two dissociatively adsorbed $H_2O$ molecules is preferred due to the high degree of hydrogen bonding with the first dissociatively adsorbed $H_2O$, which leads to the more favorable adsorption of the second water ($E_{ads}$ = −269 kJ/mol) relative to the first dissociative $H_2O$ adsorption event.

**2.2. $NH_2$* Formation.** $NH_2$* could nominally form directly by proton transfer (PT) to NH* from a dissociatively adsorbing $H_2O$ or by proton migration between two NH* sites formed by two dissociatively adsorbed $H_2O$s. Transition state (TS)

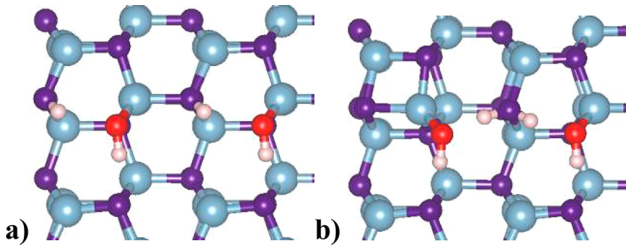


**Figure 3.** (a) Dissociative adsorption of a second $H_2O$ forms two OH*s and two NH*s. This configuration mimics the configuration described for dissociative adsorption of a single $H_2O$. (b) $NH_2$* intermediate formed by proton transfer between two neighboring NH* sites by a hydroxyl-mediated proton relay.

searches for the direct path fail to identify a low-energy TS for direct PT and instead optimize to a minimum associated with the dissociatively adsorbed state of the second $H_2O$. From this low-energy initial configuration of two dissociated $H_2O$ molecules (Figure 3a), NH2* (Figure 3b) forms through a two-step proton relay mechanism mediated by OH*, as depicted in Figure 4. In the first step, the proton of one NH* transfers to a neighboring OH* to transiently reform molecular water, $H_2O$*, at the transition state (TS1); the transient molecular water then transfers its original proton to an adjacent bare N site to form an intermediate NH* surface species. The first PT from NH* to OH* occurs along the entrance channel of the first step of the reaction, and the second PT from the transiently formed $H_2O$* to N to form the NH* intermediate occurs along its exit channel. The net result of this endothermic proton relay is to transfer an adsorbed proton from a surface NH* far from the active NH* site, where $NH_2$* will form, to a N closer to the active NH* site. From this configuration, a second PT occurs to form $NH_2$*. First, the NH* proton transfers to OH* to again transiently form $H_2O$*, and then a proton transfers from $H_2O$* to form $NH_2$*. Like the first PT step, the second PT step is mediated by OH*. The TS of this second proton relay (TS2) involves a ∼ 120° rotation of OH* to orient the transient $H_2O$* for the final PT to NH* to form $NH_2$*, although $H_2O$* can also rotate to orient its other proton for PT to NH*. In both PT steps, the TS appears to be a molecularly adsorbed state that could be a plausibly stable adsorption configuration. However, in relaxing states akin to TS1 and TS2, no stable molecular $H_2O$* states were found, instead optimizing to one of the 2NH* dissociated states shown in Figure 4. It is also plausible that the 2NH* state (Figure 3a) could form $NH_2$* (Figure 3b) directly through a larger rotation of the molecularly adsorbed state (TS1), thus bypassing the intermediate 2NH* state. However, in this potential single-step pathway, transition state TS2 is unavoidable, and thus this pathway would proceed with the same activation barrier as the two-step pathway shown in Figure 4. The two-step pathway through the 2NH* intermediate is thus shown for completeness, as the 2NH* intermediate is energetically stable relative to TS2 and $NH_2$*.

The proton relays of the first and second steps are analogous to proton transfers in aqueous and other hydrogen-bonded liquids that operate by the Grotthuss mechanism. However, in this case, the process occurs on a partially hydroxylated surface where a hydroxyl acts as the mediator that accepts and donates the transferring protons via transient $H_2O$* formation rather than within the hydrogen-bonded network of a liquid, where $H_2O$ mediates PT via transient $H_3O^+$ formation. At reaction conditions, a thin layer of physisorbed water molecules present


DOI: 10.1021/acsami.6b04375
ACS Appl. Mater. Interfaces 2016, 8, 18550−18559

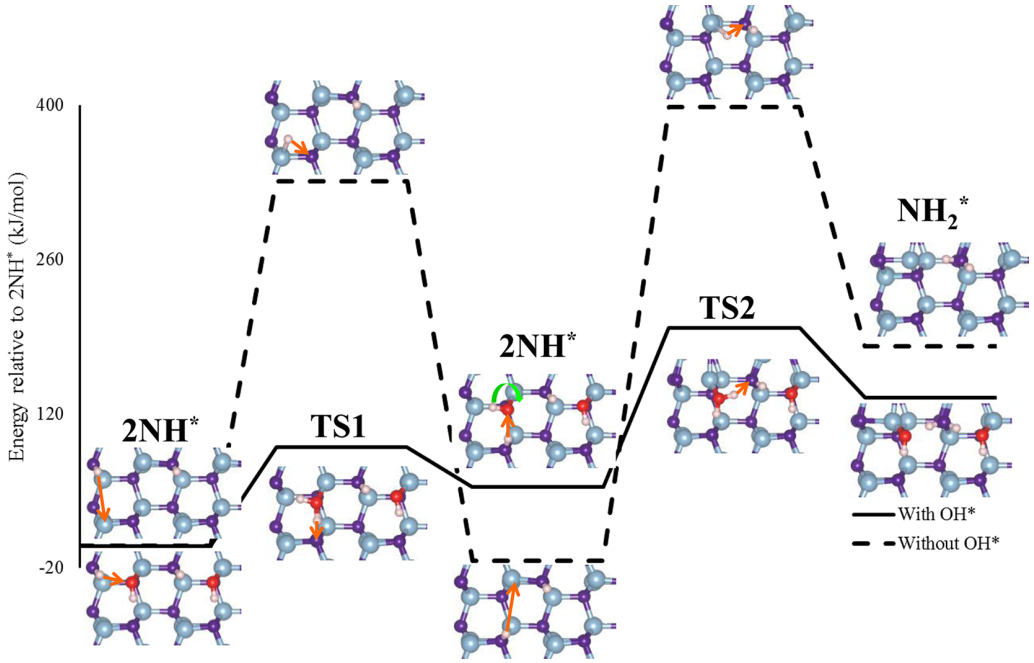


**Figure 4.** Calculated schematic potential energy surfaces for $NH_2$* formation from two neighboring NH* sites with and without proton-transfer mediation by an OH*; $NH_2$* formation mechanism where two sequential proton relay steps, each involving two sequential proton transfers, are mediated by the OH* and $NH_2$* formation mechanism in the absence of surface OH*. Proton transfer mediated by OH* substantially decreases the activation energy for both the proton "hop" to a vacant N site (TS1) and for the proton transfer to NH* to form $NH_2$* (TS2), demonstrating the ability of OH* to catalyze proton transfers and, specifically, $NH_2$* formation. A table of the energies of each stable and transition state is provided in Table S1.

near the surface may also contribute to enhanced proton diffusion through a more traditional bulk Grotthuss-like transport mechanism, where $H_2O$ mediates PT through the formation of $H_3O^+$ intermediates.

We calculated the hydroxyl-mediated PT to form $NH_2$* to be endothermic by 135 kJ/mol and to proceed over a barrier of 198 kJ/mol, as shown in Figure 4. The endothermicity of this reaction is explained by the requirement that to accommodate a second proton at the NH* site to form $NH_2$*, one of the three mostly covalent Al−NH* surface bonds must dissociate.

Aqueous-phase proton-relay mechanisms mediated by water via a Grotthuss-like mechanism have been reported to provide low-energy pathways for a number of reactions.[45−52] Although surface Grotthuss-like mechanisms where the OH* surface species mediate the PT and $H_2O$* transiently forms are less common, proton conduction mechanisms mediated by adsorbed hydroxyl groups have also been previously reported.[43,53,54] However, to the best of our knowledge, this is the first reported ab initio description of a Grotthuss-like proton transport mechanism across a solid surface mediated by immobile surface hydroxyl groups in the absence of solvation.

To further examine how the hydroxyl-mediated proton relay catalyzes the formation of $NH_2$*, we investigated $NH_2$* formation in the absence of OH*. The $NH_2$* formation barrier in this case is 412 kJ/mol (Figure 4), substantially larger than the 198 kJ/mol barrier to $NH_2$* formation mediated by the hydroxyl-mediated proton relay, also shown in Figure 4. This indicates that the adsorbed hydroxyl groups catalyze $NH_2$* formation by reducing the activation barrier to proton transport by more than 200 kJ/mol and thereby facilitate surface proton transfer. Our calculations of proton transport in the absence of OH* also provide insight into the mechanism of AlN hydrolysis. The first step of the proton transport from the more stable NH* site to the intermediate NH* site is endothermic in the presence of OH* (first step of Figure 4) but approximately thermoneutral in the absence of OH* (first step of Figure 4). This is because in the absence of OH*, all NH* sites are approximately equivalent energetically due to the absence of a hydrogen-bonding network that requires specific arrangements of the NH* and OH* surface groups to maximize stability. Consequently, the endothermicity for this first step in the presence of OH* arises from the loss of hydrogen bonding due to the transfer of a proton from the most-favorable N site to a less-favorable site, although the proton relay results in a different proton occupying the intermediate NH* site than the proton that occupied the initial, lower energy NH* site.

In the second step of the reaction to form $NH_2$*, we calculate that the transport of the proton to form $NH_2$* is endothermic both in the presence and absence of OH* (second steps of Figure 4). Therefore, this endothermicity cannot stem solely from the loss of hydrogen bonding because no hydrogen bonding exists in the absence of OH*. The formation of the $NH_2$* intermediate requires that a surface N, which was initially bonded to three neighboring Al atoms, breaks an Al−N bond to accommodate the second proton because a 5-fold coordinated N would involve a prohibitively high-energy rehybridization. Thus, the endothermic nature of the second proton relay step results from the dissociation of the mostly covalent Al−N surface bond to form $NH_2$*. Figure 4 illustrates that the overall presence of OH* reduces the activation barrier required to transport protons across the AlN surface by more than 200 kJ/mol. Our results are unique in demonstrating the mechanism by which OH* formed by $H_2O$ dissociative adsorption mediates the transport of protons across a metal


DOI: 10.1021/acsami.6b04375
ACS Appl. Mater. Interfaces 2016, 8, 18550−18559

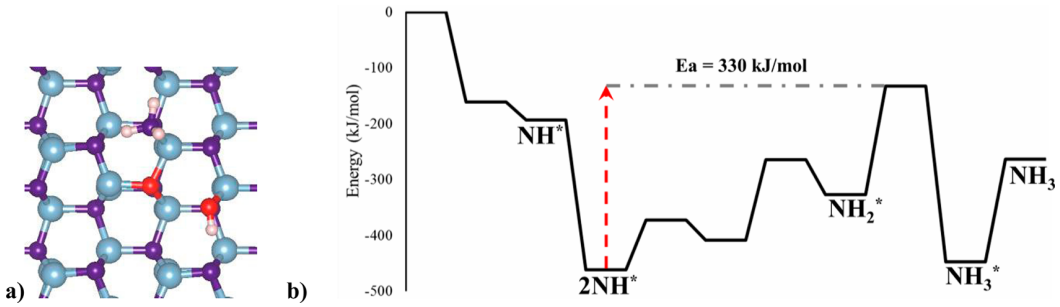


**Figure 5.** (a) Structure of the $NH_3$* surface site that forms from the reaction between OH* and $NH_2$*. The formation of $NH_3$* forms a N vacancy in the AlN surface that is filled by the O atom from dissociating OH*, which provides the proton. (b) Schematic potential energy surface for $NH_3$ formation and desorption through the "two-water" mechanism. Each labeled structure is illustrated in the following figures: NH* (Figure 2b); 2NH* (Figure 3a); NH* (Figure 3b); and NH* (Figure 5a). A table of the energies of each stable and transition state shown in Figure 5b is provided in Table S2.

nitride surface in the absence of solvation through the formation of an adsorbed $H_2O$* intermediate. This differs from previously demonstrated proton hopping mechanisms on metal oxides, where proton hopping is mediated either by solvating water molecules that form $H_3O^+$ intermediates[44] or through adsorption into oxygen vacancies within the native oxide, resulting in mobile OH and $H_2O$ species within the surface layer.[42,43]

We also considered the propensity to form an $NH_2$* intermediate from the single dissociated water structure depicted in Figure 2b. However, we found that the formation of a stable $NH_2$* intermediate from a single water is too unfavorable for a surface N to form two NH* bonds (thus breaking one Al−N bond) in the presence of a neighboring O* adatom. That is, the Al−OH* + (3Al)−NH* state is significantly more favorable than the Al−O* + (2Al)−$NH_2$* state.

**2.3. $NH_3$ Formation by Proton Migration Involving Two Adsorbed Waters: "Two-Water Case".** Subsequent to the $NH_2$* formation (Figure 4) described previously, a third proton must transfer from a neighboring OH* to the $NH_2$* to produce $NH_3$*. The two-water case described here involves only two dissociated $H_2O$*s, but alternative pathways involving additional dissociatively adsorbed $H_2O$ molecules are also possible and will be discussed below. For $NH_2$* to accommodate the third proton and form $NH_3$*, it must break another Al−N bond, analogous to the dissociation of an Al−N bond to accommodate the second proton in the formation of $NH_2$* that avoids high-energy 5-fold coordinated N. Dissociation of the second Al−N bond causes $NH_3$* to relax away from the surface as it becomes a molecularly adsorbed species, now bonded to a single Al through an Al−N bond of primarily dative character (Figure 5a). This step to form $NH_3$* generates a transient N vacancy in the surface. The two-water mechanism to form $NH_3$* involves PT from the neighboring OH* to $NH_2$* to form $NH_3$*, and the resulting O adatom concomitantly relaxes into the transiently formed surface N vacancy, as shown in Figure 5a. As the O−H bond of OH* dissociates, the O atom forms two Al−O bonds of mixed covalent−dative character. We calculate that this partially concerted step is exothermic by 120 kJ/mol, with an activation barrier of 195 kJ/mol.

Although the dissociation of an Al−N bond to form $NH_3$* involves an energy penalty equal to the Al−N bond strength, the partially concerted step is net exothermic as a result of the formation of the N−H bond and the two additional Al−O bonds that form as O fills the N vacancy. Despite the moderately exothermic nature of this step, it involves a relatively large 195 kJ/mol barrier. This is because this step involves the dissociation (O−H and Al−N bonds) and formation (N−H, two Al−O bonds) of several bonds where the high-energy Al−N bond dissociations occur before the O can fill the vacancy. This step occurs sequentially because the N must first vacate its position to form the vacancy, which can then be filled by the O adatom. Because the two Al−O bonds form subsequent to the dissociation of the O−H and Al−N bonds, a late transition state arises where the two bond dissociations are relatively decoupled from the formation of the two Al−O bonds that cause this step to be exothermic. This step establishes a mechanism that concomitantly forms $NH_3$* and introduces oxygen into the AlN lattice during the initial hydrolysis of AlN. The overall pathway from the state with two adsorbed waters (2NH*, Figure 3a) to the molecularly adsorbed $NH_3$* state (Figure 5a) has an activation barrier of 330 kJ/mol (Figure 5b). The magnitude of this barrier agrees with the experimental observation that hydrolysis of AlN is slow under conditions where AlN is exposed to steam below 950 °C.[26,29] We attribute this relatively large activation barrier to the successive dissociation of strong Al−N bonds at the surface to liberate N from the AlN lattice. We note that reporting a single activation barrier for three successive elementary steps will not capture the kinetic details of this reaction. Alternatively, a kinetic Monte Carlo model based on our predicted energetics could more completely describe the overall reaction kinetics, but this is beyond the scope of this work. The energies of each stable and transition state shown in Figure 5b can be found in Table S2.

The desorption of $NH_3$* involves the dissociation of the Al−N bond between the molecularly adsorbed $NH_3$* and the Al surface site to which it is bound and is calculated to be endothermic by 184 kJ/mol. This relatively large endothermicity is due to dissociation of the third and final Al−N bond, which is stronger than might be expected on the basis of a surface dative bond and the energy required to form $NH_2$ because although the Al−N bond is nominally a dative bond, it is partially covalent in character. This increased covalency arises from the fact that the surface Al to which the $NH_3$ is bound is also bound to a 3-fold coordinated O. This O atom provides additional electron density to the Al atom, increasing the dative character of the Al−O bond and thus increasing the covalent character of the Al−N bond to $NH_3$*, which consequently decreases the covalent character of two of the N−H bonds.


DOI: 10.1021/acsami.6b04375
ACS Appl. Mater. Interfaces 2016, 8, 18550−18559

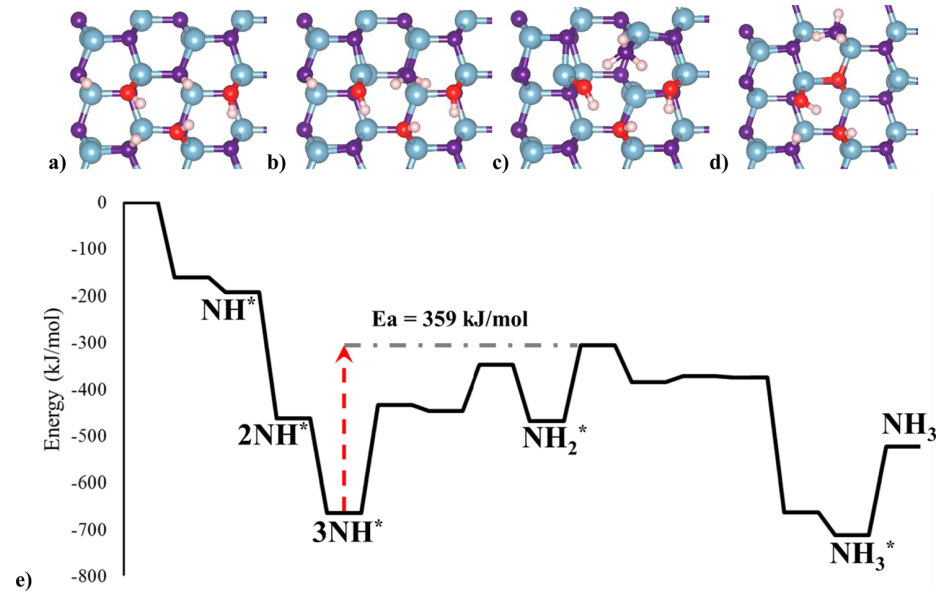


**Figure 6.** (a) 3NH* resulting from the dissociative adsorption of three $H_2O$ molecules. (b) $NH_2$* formed from a hydroxyl-mediated proton relay. (c) $NH_3$* and a transiently formed N surface vacancy. (d) $NH_3$* following filling of the N vacancy by O that leads to surface oxidation. (e) $NH_3$ formation and desorption pathway for the three-water mechanism. NH* (Figure 2b); 2NH* (Figure 3a); 3NH* (Figure 6a); NH2* (Figure 6b); and NH3* (Figure 6d). A table of the energies of each stable and transition state shown in Figure 6e is provided in the Table S3.

This is exhibited by the lengthening of two of the N−H bonds of $NH_3$*, where two are 1.04 Å long and the third is 1.02 Å long. The N−H bond of desorbed $NH_3$ is calculated to be 1.02 Å, illustrating that two of the N−H bonds of $NH_3$* have decreased covalent character, enabling the strengthened Al−N bond.

**2.4. $NH_3$ Formation with an Additional Adsorbed $H_2O$: "Three-Water Case".** Having elucidated the initial AlN hydrolysis mechanism of AlN oxidation and $NH_3$ liberation for the case involving the minimum number of dissociated $H_2O$ molecules, we next investigated potential hydrolysis pathways involving additional dissociatively adsorbed $H_2O$ that would be present at higher coverages of $H_2O$. For the simplest case of hydrolysis with additional water present, we modeled the adsorption and dissociation of a third $H_2O$ (Figure 6a) to the surface with the minimum-energy 2NH* configuration resulting from two dissociatively adsorbed $H_2O$ molecules (Figure 3a). The third $H_2O$ molecule was predicted to adsorb to the surface with an adsorption energy of −202 kJ/mol, falling between the adsorption energies of the first and second dissociatively adsorbed $H_2O$ molecules. The added energetic benefit of hydrogen bonding of this adsorbed $H_2O$ to neighboring NH* and OH* groups on the surface leads to a slightly more-favorable adsorption than the first water. However, steric effects and lattice strain as a result of the increased coverage of OH* and NH* on the surface diminish the energetic benefit of the additional hydrogen bonding, as compared to the adsorption of the second water.

The formation of $NH_2$* (Figure 6b) is analogous to the mechanism we predicted for the two-water case (Figure 4); we calculated that $NH_2$* is again formed by an endothermic hydroxyl-mediated proton relay. However, for this case, we calculated that the formation of $NH_2$* is more endothermic and kinetically unfavorable than for the corresponding two-water reaction, with an endothermicity and activation barrier of 196 and 317 kJ/mol, respectively. The larger endothermicity and barrier are attributed to the additional hydrogen bonds of the denser hydrogen bond network that must be disrupted in the three-water case relative to the two-water case. Additionally, steric effects caused by the higher coverage of adsorbed $H_2O$ hinder the dissociation of the Al−N bond that accompanies $NH_2$* formation.

From the $NH_2$* state, we again predict that $NH_3$* (Figure 6c) is formed from a hydroxyl-mediated proton relay, as in the two-water case. However, because the hydrogen-bonding network has already been locally disrupted in the process of forming $NH_2$*, this step was calculated to be substantially less-unfavorable than $NH_2$* formation, with an endothermicity and activation barrier of 83 and 162 kJ/mol, respectively. In contrast to the two-water case where $NH_3$* formation is coupled with surface oxidation, $NH_3$* forms via a two-step mechanism in the three-water case; $NH_3$* is first formed by a proton relay from NH*. In this case, each of the three dissociatively adsorbed $H_2O$s provide one proton to form $NH_3$*, three OH* intermediates, and a surface N vacancy. This structure is stabilized by significant hydrogen bonding, and its N vacancy is filled by an O atom provided by a neighboring OH* through a concerted PT from the OH* to a neighboring OH* to form $H_2O$* (Figure 6d). This provides a low-energy pathway to form $NH_3$* and the associated intermediate N vacancy and to subsequently fill the N vacancy. Examination of the structure of the N vacancy (Figure 6c) shows that in the case of additional water, the additional OH* groups on the surface hydrogen bond with the newly formed $NH_3$* to effectively hinder it from relaxing fully to its top position above a surface Al atom. The relaxation of $NH_3$* to the top position enables the exothermic oxidation of the AlN surface by a neighboring OH* group, which readily transfers its proton to another neighboring OH* in the process of filling the vacancy (Figure 6d). Finally, $NH_3$* desorbs with a desorption energy of 189 kJ/mol, nearly identical to that predicted for the two-water case, which should be expected given that the adsorbed $NH_3$* that results after the oxidation step does not form H bonds with


DOI: 10.1021/acsami.6b04375
ACS Appl. Mater. Interfaces 2016, 8, 18550−18559

any neighboring adsorbates and thus appears analogous to the adsorbed $NH_3$* of the two-water case.

The schematic potential energy surface for the complete pathway from 3NH* and 3OH* to desorbed $NH_3$, and an oxidized surface site is shown in Figure 6e and was calculated to have an activation barrier of 359 kJ/mol. This barrier is comparable to that seen in the two-water case (330 kJ/mol), although it is slightly larger as a result of the required dissociation of additional hydrogen bonds in the denser hydrogen bonding network associated with the 3NH* + 3OH* state compared with the 2NH* + 2OH* state of the two-water case. Comparing the two-water and three-water pathways, we find that the mechanisms are similar. In both cases, it is the dissociation of the two Al−N bonds that are required for the accumulation of three protons at a surface N that gives rise to the large barriers associated with hydrolyzing AlN. These large barriers to liberating nitrogen from the AlN lattice explain the slow initial conversion of AlN into $NH_3$ and $Al_2O_3$ by hydrolysis at moderate temperatures (<950 °C). As mentioned in the discussion of the two-water pathway, a more rigorous analysis of the reaction kinetics could involve the construction of a kinetic Monte Carlo model, which was deemed outside the scope of this work.

Our analysis does not consider the continued hydrolysis of AlN, which likely involves the formation of an oxynitride (Al−O−N) and ultimately an $Al_2O_3$ film on the surface and the diffusive transport of $O^{2-}$ and $N^{3-}$ ions through the oxide film of the oxidizing particle. We instead focused on the initial steps, which introduce oxygen into the AlN lattice that begin the liberation of N in the form of $NH_3$. The results of our theoretical work indicate that a large barrier (~350 kJ/mol) is associated with the initial surface reactions that must occur at the onset of AlN hydrolysis and $NH_3$ liberation. The barriers calculated for $NH_3$ formation from AlN of approximately 350 kJ/mol are considerably larger than would be expected for a solid-state diffusion process,[55,56] suggesting that the rate-determining step of the initial hydrolysis of AlN is the initial reaction at the surface and not the diffusion through the oxidizing particle. This may also be true for subsequent oxidation of the partially oxidized AlN particle, which possesses a core−shell structure with an Al−O−N film, where oxidation presumably involves analogous reactions to form $NH_3$ from N atoms at the surface. However, we note that a first-principles elucidation of the detailed mechanism and energetics becomes complicated after the initial hydrolysis of the bare AlN surface, where a large number of possible structures of the partially oxidized surface are possible and solid-state diffusion begins to play a large role. Additionally, the dissociation of $NH_3$ into $N_2$ and $H_2$ may become relevant at elevated temperatures and at the later stages of hydrolysis. This work is a first step in understanding this complex process but does not purport to describe the later stages of AlN hydrolysis, where the surface is less well-defined and where solid-state diffusion and $NH_3$ decomposition may play a larger role.

## 3. CONCLUSIONS

We have performed ab initio quantum chemical calculations on plausible pathways for the hydrolysis of the $(1\bar{1}\ 00)$ surface of wurtzite AlN. First, we considered six unique $H_2O$ adsorption geometries to identify the lowest energy configuration of dissociatively adsorbed $H_2O$. $H_2O$ that dissociatively adsorbs to the AlN surface to form N−H* + Al−OH* is the most stable of those evaluated. Subsequently, reaction paths involving a second adsorbed $H_2O$ were considered for the formation of the $NH_2$* intermediate. The $NH_2$* intermediate forms via a surface hydroxyl-mediated proton-relay mechanism, which is a surface Grotthuss-like proton relay where adsorbed hydroxyls act to mediate the proton relay. The formation of $NH_2$* is accompanied by the dissociation of one of the three Al−N bonds at the NH* center. In this analysis, we also identify the dissociation of predominantly covalent Al−N bonds as the primary cause of the large barriers that results in the kinetic challenge of liberating nitrogen from AlN by hydrolysis in the case of thermochemical $NH_3$ generation. From the $NH_2$* intermediate, we find a similar Grotthuss-like mechanism for $NH_2$* formation. During the proton migration through the proton relay and the Al−N bond dissociation step, we predict that a N vacancy is formed, which is subsequently filled by a surface O. In the case of low $H_2O$ coverage, this step is partially concerted where the N vacancy forms transiently as it is concomitantly filled by an O surface atom and $NH_3$ forms. We elucidate a similar mechanism for the case of additional water present on the AlN surface. In the case of higher $H_2O$ coverage, the $NH_3$ generation step involves the formation of an intermediate N vacancy and $NH_3$*, where the N vacancy is subsequently filled by a surface O atom.

We calculate activation barriers for the overall hydrolysis reaction to be 330 or 359 kJ/mol for minimal water coverage and additional water coverage cases, respectively. These results are corroborated by previous experimental work that demonstrated that little or no conversion of AlN to $NH_3$ occurs below 950 °C. In the elucidation of this mechanism and the associated energetics, we present an enhanced understanding of the behavior of AlN and, more broadly, metal nitrides when exposed to water, thereby oxidizing and liberating nitrogen as $NH_3$. These results have important implications for designing processes that either avoid oxidation by hydrolysis (for example, in the case of processing AlN powder for thermal-management applications) or for designing materials that possess favorable thermodynamics and kinetics for solar thermal redox processes using metal nitrides to efficiently generate carbon-free $NH_3$. In the search for metal nitrides with fast-oxidation kinetics for carbon-free $NH_3$ synthesis, it is important to consider the metal−nitrogen bond strength, which can be correlated to the metal−oxygen bond strength of the accompanying oxide. The mechanism we predict for AlN hydrolysis involves nitrogen liberation in the form of $NH_3$ and large activation barriers associated with the dissociation of mostly covalent Al−N bonds, which explains the slow experimentally observed hydrolysis kinetics. However, a metal nitride with metal−nitrogen bonds with less covalent character will result in lower activation barriers to $NH_3$ generation and thus improved hydrolysis kinetics.

## 4. METHODS

Plane-wave periodic-boundary-condition DFT calculations were performed using the Vienna Ab Initio Simulation Package.[57,58] All calculations employed the Perdew−Burke−Ernzerhof (PBE) generalized gradient approximation (GGA) exchange and correlation functional[59] coupled with projector augmented wave (PAW) pseudopotentials.[60] For these calculations, PAWs were used to explicitly describe the aluminum 3s and 3p; nitrogen 2s and 2p; oxygen 2s and 2p; and hydrogen 1s electrons. A 96 atom, 2 × 2 supercell of the $(1\bar{1}\ 00)$ surface of wurtzite AlN was used as the model for the reacting surface. This crystal structure was chosen because Schmerler et al. showed that the wurtzite phase is the stable structure at the conditions of interest for electrical and $NH_3$ generation


DOI: 10.1021/acsami.6b04375
ACS Appl. Mater. Interfaces 2016, 8, 18550−18559

applications.[61] The lattice constants computed in this work match those obtained previously by both the experiment and the calculation to within 1% (Table 1). Of the low-index facets of wurtzite AlN, Holec et al. showed that by far the lowest surface energy facet is the $(1\bar{1}\,00)$ surface.[62] The 96 atom slab consists of six AlN layers and has a thickness of 9.4 Å in a 24.4 Å thick supercell, meaning that 15 Å of vacuum space separates the reacting surface from the bottom layer of the adjacent slab (see Figure 1). To obtain the model surface, we allowed the bulk AlN wurtzite structure to fully relax, added vacuum space, and then allowed the top four layers of the slab to relax while the bottom two layers were frozen to mimic the bulk subsurface. All calculations utilized a 450 eV cutoff energy based on a cutoff energy convergence study over the range of 250−500 eV, where a 450 eV cutoff energy was found to produce a total energy within 0.01 eV/supercell of that produced with a 500 eV cut-off energy. The slab was relaxed using various Monkhorst−Pack k-point meshes between 1 × 1 × 1 and 6 × 6 × 1, where the 3 × 3 × 1 k-point grid produced energies within 0.01 eV per supercell of those computed using the finer and more computationally demanding meshes. Bader charge analyses were conducted using software from the Henkelman group.[63−65] All reaction-energy barriers were obtained using the climbing-image nudged-elastic-band (cNEB) method[66,67] or a combination of cNEB and the Dimer method.[68] All geometries, including cNEB images, were relaxed until the magnitude of the maximum force on the optimized ions was less than 0.03 eV/Å. Adsorption energies were calculated using eq 3:

$$E_{ads} = E_{surf,mol} - E_{surf} - E_{mol} \quad (3)$$

where $E_{ads}$ is the energy of adsorption, $E_{surf}$ is the energy of the perfect surface, $E_{mol}$ is the energy of the isolated adsorbing molecule in vacuum, and $E_{surf,mol}$ is the energy of the surface with the adsorbate.

**Table 1. Lattice Constants Compared to Previously Published Values**

| lattice constant[a] | this work (Å) | previous calculation (Å)[69] | previous experiment (Å)[70] |
|---|---|---|---|
| $a$ | 3.14 | 3.12 | 3.11 |
| $c$ | 5.00 | 5.00 | 4.98 |

[a]For wurtzite, $a = b \neq c$.

## ■ ASSOCIATED CONTENT

### Supporting Information

The Supporting Information is available free of charge on the ACS Publications website at DOI: 10.1021/acsami.6b04375.

Tables showing the energies of all stable and transitions states shown in Figures 4, 5b, and 6e. (PDF)

96 atom AlN slab (CIF)

## ■ AUTHOR INFORMATION


### Corresponding Authors

*A.W.W. e-mail: alan.weimer@colorado.edu.

*C.B.M. e-mail: charles.musgrave@colorado.edu.


### Notes

The authors declare no competing financial interest.

## ■ ACKNOWLEDGMENTS

This material is based upon work supported by the National Science Foundation Graduate Research Fellowship under grant DGE 114083. C.B.M. was partially supported by the National Science Foundation (NSF award no. CBET-1433521). This work utilized the Janus supercomputer, which is supported by the National Science Foundation (award no. CNS-0821794), the University of Colorado Boulder, the University of Colorado Denver, and the National Center for Atmospheric Research. The Janus supercomputer is operated by the University of Colorado Boulder.

## ■ REFERENCES


(1) Slack, G. A.; Tanzilli, R. A.; Pohl, R. O.; Vandersande, J. W. The Intrinsic Thermal Conductivity of AlN. *J. Phys. Chem. Solids* **1987**, *48* (7), 641−647.

(2) Mohammed, A. C.; Corbett, S. J. Thick Film Metallizations and Performance of a Power Hybrid Module on Aluminum Nitride Substrates. In *Proceedings of the International Symposium on Microelectronics, International Society of Hybrid Microelectronics*, Anaheim, CA, November 11−14, 1985; International Society for Hybrid Microelectronics: Reston, VA, 1985; 218.

(3) Watari, K.; Hwang, H. J.; Toriyama, M.; Kanzaki, S. Effective Sintering Aids for Low- Temperature Sintering of AlN Ceramics. *J. Mater. Res.* **1999**, *14* (4), 1409−1417.

(4) Weimer, A. W. *Carbide, Nitride and Boride Materials Synthesis and Processing*; Springer: The Netherlands, 1997; p 696.

(5) Werdecker, W.; Aldinger, F. Aluminum Nitride - An Alternatice Ceramic Substrate for High Power Applications in Microcircuits. *IEEE Trans. Compon., Hybrids, Manuf. Technol.* **1984**, *7* (4), 399−404.

(6) Kuramoto, N.; Taniguchi, H. Fine Powder of Aluminum Nitride, Composition and Sintered Body Thereof and Processes for Their Production. U.S. Patent 4,618,592, Oct 21, 1986.

(7) Weimer, A. W.; Cochran, G. A.; Eisman, G. A.; Henley, J. P.; Hook, B. D.; Mills, L. K.; Guiton, T. A.; Knudsen, A. K.; Nicholas, R. N.; Volmering, J. E.; Moore, W. G. Rapid Process for Manufacturing Aluminum Nitride Powder. *J. Am. Ceram. Soc.* **1994**, *77* (1), 3−18.

(8) Katila, P. UV and Industrial LED Applications Require Efficient Thermal Substrates. *LEDs Magazine*, March 23, 2015.

(9) Harris, J. Cost-Reduced AlN Delivers Thermals Needed in HBLED Packages. *LEDs Magazine*, September 2013, 2013.

(10) Moore, A. L.; Shi, L. Emerging Challenges and Materials for Thermal Management of Electronics. *Mater. Today* **2014**, *17* (4), 163−174.

(11) Bardsely, N.; Bland, S.; Chwastyk, D.; Pattison, L.; Pattison, M.; Stober, K.; Yamada, M. *Manufacturing Roadmap: Solid-State Lighting Research and Development*; United States Department of Energy: Energy Efficiency & Renewable Energy: Washington, DC, 2014; pp 1−127.

(12) Shimizu, Y.; Hatano, J.; Hyodo, T.; Egashira, M. Ion-Exchange Loading of Yttrium Acetate as a Sintering Aid on Aluminum Nitride Powder via Aqueous Processing. *J. Am. Ceram. Soc.* **2000**, *83* (11), 2793−2797.

(13) de Baranda, P. S.; Knudsen, A. K.; Ruh, E. Effect of Yttria on the Thermal Conductivity of Aluminum Nitride. *J. Am. Ceram. Soc.* **1994**, *77* (7), 1846−1850.

(14) Troczynski, T. B.; Nicholson, P. S. Effect of Additives on the Pressureless Sintering of Aluminum Nitride between 1500 and 1800 degrees C. *J. Am. Ceram. Soc.* **1989**, *72* (8), 1488−1491.

(15) Slack, G. A. Nonmetallic Crystals with High Thermal Conductivity. *J. Phys. Chem. Solids* **1973**, *34*, 321−335.

(16) Virkar, A. V.; Jackson, T. B.; Cutler, R. A. Thermodynamic and Kinetic Effects of Oxygen Removal on the Thermal Conductivity of Aluminum Nitride. *J. Am. Ceram. Soc.* **1989**, *72* (11), 2031−2042.

(17) Ganesh, I.; Thiyagarajan, N.; Sundararajan, G.; Olhero, S. M.; Ferreira, J. M. F. A Non-Aqueous Processing Route for Phosphate-Protection of AlN Powder Against Hydrolysis. *J. Eur. Ceram. Soc.* **2008**, *28* (11), 2281−2288.

(18) Tanaka, S.; Hojo, F.; Kagawa, H.; Takezawa, Y. Fabrication of Highly Water-Resistant AlN Particles with Hybrid alpha-$Al_2O_3$/Organic Layers. *J. Ceram. Soc. Jpn.* **2014**, *122* (1423), 211−215.

(19) Egashira, M.; Shimizu, Y.; Takatsuki, S. Chemical Surface Treaments of Aluminum Nitride Powder Suppressing its Reactivity With Water. *J. Mater. Sci. Lett.* **1991**, *10*, 994−996.




DOI: 10.1021/acsami.6b04375
*ACS Appl. Mater. Interfaces* 2016, 8, 18550−18559

(20) Morisada, Y.; Sakurai, T.; Miyamoto, Y. A New Water-Resistant Coating for AlN Powders. *Int. J. Appl. Ceram. Technol.* **2004**, *1* (4), 374−380.
(21) Oliveira, M.; Olhero, S.; Rocha, J.; Ferreira, J. M. F. Controlling Hydrolysis and Dispersion of AlN Powders in Aqueous Media. *J. Colloid Interface Sci.* **2003**, *261* (2), 456−463.
(22) Hellman, A.; Baerends, E. J.; Biczysko, M.; Bligaard, T.; Christensen, C. H.; Clary, D. C.; Dahl, S.; van Harrevelt, R.; Honkala, K.; Jonsson, H.; Kroes, G. J.; Luppi, M.; Manthe, U.; Nørskov, J. K.; Olsen, R. A.; Rossmeisl, J.; Skúlason, E.; Tautermann, C. S.; Varandas, A. J. C.; Vincent, J. K. Predicting Catalysis: Understanding Ammonia Synthesis from First-Principles Calculations. *J. Phys. Chem. B* **2006**, *110* (36), 17719−17735.
(23) Kirova-Yordanova, Z. Exergy Analysis of Industrial Ammonia Synthesis. *Energy* **2004**, *29* (12), 2373−2384.
(24) Ritter, S. K. The Haber-Bosch Reaction: An Early Chemical Impact on Sustainability. *Chem. Eng. News* Aug 18, 2008; *86* (33).
(25) Muhich, C. L.; Ehrhart, B. D.; Al-Shankiti, I.; Ward, B. J.; Musgrave, C. B.; Weimer, A. W. A Review and Perspective of Efficient Hydrogen Generation via Solar Thermal Water Splitting. *Wiley Interdiscip. Rev.: Energy Environ.* **2016**, *5*, 261.
(26) Gálvez, M. E.; Frei, A.; Halmann, M.; Steinfeld, A. Ammonia Production via a Two-Step $Al_2O_3$/AlN Thermochemical Cycle. 2. Kinetic Analysis. *Ind. Eng. Chem. Res.* **2007**, *46* (7), 2047−2053.
(27) Michalsky, R.; Avram, A. M.; Peterson, B. A.; Pfromm, P. H.; Peterson, A. A. Chemical Looping of Metal Nitride Catalysts: Low-Pressure Ammonia Synthesis for Energy Storage. *Chemical Science* **2015**, *6*, 3965−3974.
(28) Michalsky, R.; Parman, B. J.; Amanor-Boadu, V.; Pfromm, P. H. Solar Thermochemical Production of Ammonia from Water, Air and Sunlight: Thermodynamic and Economic Analyses. *Energy* **2012**, *42* (1), 251−260.
(29) Michalsky, R.; Pfromm, P. H. An Ionicity Rationale to Design Solid Phase Metal Nitride Reactants for Solar Ammonia Production. *J. Phys. Chem. C* **2012**, *116* (44), 23243−23251.
(30) Michalsky, R.; Pfromm, P. H. Thermodynamics of Metal Reactants for Ammonia Synthesis from Steam, Nitrogen and Biomass at Atmospheric Pressure. *AIChE J.* **2012**, *58* (10), 3203−3213.
(31) Michalsky, R.; Pfromm, P. H.; Steinfeld, A. Rational Design of Metal Nitride Redox Materials for Solar-driven Ammonia Synthesis. *Interface Focus* **2015**, *5* (3), DOI: 2014008410.1098/rsfs.2014.0084.
(32) Michalsky, R.; Pfromm, P. H. Chromium as Reactant for Solar Thermochemical Synthesis of Ammonia from Steam, Nitrogen, and Biomass at Atmospheric Pressure. *Sol. Energy* **2011**, *85* (11), 2642−2654.
(33) Fukumoto, S.; Hookabe, T.; Tsubakino, H. Hydrolysis Behavior of Aluminum Nitride in Various Solutions. *J. Mater. Sci.* **2000**, *35*, 2743−2748.
(34) Heyns, A. M.; Prinsloo, L. C.; Range, K.-J.; Stassen, M. The Vibrational Spectra and Decomposition of $\alpha$-Calcium Nitride ($\alpha$-$Ca_3N_2$) and Magnesium Nitride ($Mg_3N_2$). *J. Solid State Chem.* **1998**, *137* (1), 33−41.
(35) Bowen, P.; Highfield, J. G.; Mocellin, A.; Ring, T. A. Degradation of Aluminum Nitride Powder in an Aqueous Environment. *J. Am. Ceram. Soc.* **1990**, *73* (3), 724−728.
(36) Oue, M.; Inagaki, K.; Yamauchi, K.; Morikawa, Y. First-principles theoretical study of hydrolysis of stepped and kinked Ga-terminated GaN surfaces. *Nanoscale Res. Lett.* **2013**, *8* (1), 232.
(37) Cortright, R. D.; Davda, R. R.; Dumesic, J. A. Hydrogen from catalytic reforming of biomass- derived hydrocarbons in liquid water. *Nature* **2002**, *418* (6901), 964−967.
(38) Ait-Ichou, I.; Formenti, M.; Pommier, B.; Teichner, S. J. Photocatalytic dehydrogenation of isopropanol on $Pt/TiO_2$ catalysts. *J. Catal.* **1985**, *91* (2), 293−307.
(39) Cheng, H.; Chen, L.; Cooper, A. C.; Sha, X.; Pez, G. P. Hydrogen spillover in the context of hydrogen storage using solid-state materials. *Energy Environ. Sci.* **2008**, *1* (3), 338−354.
(40) Feng, K.; Tang, B.; Wu, P. Selective Growth of $MoS_2$ for Proton Exchange Membranes with Extremely High Selectivity. *ACS Appl. Mater. Interfaces* **2013**, *5* (24), 13042−13049.
(41) Li, S.-C.; Chu, L.-N.; Gong, X.-Q.; Diebold, U. Hydrogen Bonding Controls the Dynamics of Catechol Adsorbed on a $TiO_2$(110). *Science* **2010**, *328* (5980), 882−884.
(42) Li, S.-C.; Zhang, Z.; Sheppard, D.; Kay, B. D.; White, J. M.; Du, Y.; Lyubinetsky, I.; Henkelman, G.; Dohnálek, Z. Intrinsic Diffusion of Hydrogen on Rutile $TiO_2$(110). *J. Am. Chem. Soc.* **2008**, *130* (28), 9080−9088.
(43) Wendt, S.; Matthiesen, J.; Schaub, R.; Vestergaard, E. K.; Lægsgaard, E.; Besenbacher, F.; Hammer, B. Formation and Splitting of Paired Hydroxyl Groups on Reduced TiO2(110). *Phys. Rev. Lett.* **2006**, *96* (6), 066107.
(44) Merte, L. R.; Peng, G.; Bechstein, R.; Rieboldt, F.; Farberow, C. A.; Grabow, L. C.; Kudernatsch, W.; Wendt, S.; Lægsgaard, E.; Mavrikakis, M.; Besenbacher, F. Water-Mediated Proton Hopping on an Iron Oxide Surface. *Science* **2012**, *336* (6083), 889−893.
(45) Lim, C. H.; Holder, A. M.; Musgrave, C. B. Mechanism of Homogeneous Reduction of $CO_2$ by Pyridine: Proton Relay in Aqueous Solvent and Aromatic Stabilization. *J. Am. Chem. Soc.* **2013**, *135* (1), 142−54.
(46) Motta, A.; Gaigeot, M. P.; Costa, D. Ab Initio Molecular Dynamics Study of the AlOOH Boehmite/Water Interface: Role of Steps in Interfacial Grotthus Proton Transfers. *J. Phys. Chem. C* **2012**, *116* (23), 12514−12524.
(47) Vassilev, P.; Koper, M. T. M.; van Santen, R. A. Ab Initio Molecular Dynamics of Hydroxyl− Water Coadsorption on Rh(1 1 1). *Chem. Phys. Lett.* **2002**, *359* (3−4), 337−342.
(48) Bianco, R.; Hay, P. J.; Hynes, J. T. Theoretical Study of O−O Single Bond Formation in the Oxidation of Water by the Ruthenium Blue Dimer. *J. Phys. Chem. A* **2011**, *115* (27), 8003−8016.
(49) Lim, C.-H.; Holder, A. M.; Hynes, J. T.; Musgrave, C. B. Reduction of $CO_2$ to Methanol Catalyzed by a Biomimetic Organo-Hydride Produced from Pyridine. *J. Am. Chem. Soc.* **2014**, *136* (45), 16081−16095.
(50) Lim, C.-H.; Holder, A. M.; Hynes, J. T.; Musgrave, C. B. Catalytic Reduction of $CO_2$ by Renewable Organohydrides. *J. Phys. Chem. Lett.* **2015**, *6* (24), 5078−5092.
(51) Kang, J. K.; Musgrave, C. B. The Mechanism of $HF/H_2O$ Chemical Etching of $SiO_2$. *J. Chem. Phys.* **2002**, *116* (1), 275−280.
(52) Li, P.; Henkelman, G.; Keith, J. A.; Johnson, J. K. Elucidation of Aqueous Solvent-Mediated Hydrogen-Transfer Reactions by ab Initio Molecular Dynamics and Nudged Elastic-Band Studies of $NaBH_4$ Hydrolysis. *J. Phys. Chem. C* **2014**, *118* (37), 21385−21399.
(53) Achtyl, J. L.; Unocic, R. R.; Xu, L.; Cai, Y.; Raju, M.; Zhang, W.; Sacci, R. L.; Vlassiouk, I. V.; Fulvio, P. F.; Ganesh, P.; Wesolowski, D. J.; Dai, S.; van Duin, A. C. T.; Neurock, M.; Geiger, F. M. Aqueous Proton Transfer Across Single-Layer Graphene. *Nat. Commun.* **2015**, *6*, 6539.
(54) Caldararu, M.; Chihaia, V.; Sohlberg, K.; Munteanu, C.; Hornoiu, C.; Carata, M. Water and Proton Mobility on g-Alumina and Sn/g-Alumina: A Combined Electrical Conductivity and Semi-empirical PM3 Study. *Prog. Catal* **2005**, *14* (1−2), 9−20.
(55) Gillot, B.; El Guendouzi, M.; Laarj, M. Particle Size Effects on the Oxidation−Reduction Behavior of $Mn_3O_4$ Hausmannite. *Mater. Chem. Phys.* **2001**, *70* (1), 54−60.
(56) Oijerholm, J. *Ionic Transport in Metal Oxides Studied in situ by Impedance Spectroscopy and Cyclic Voltammetry*; Royal Institute of Technology: Stockholm, Sweden, 2007.
(57) Kresse, G.; Furthmuller, J. Efficiency of ab-initio Total Energy Calculations for Metals and Semiconductors Using a Plane-Wave Basis Set. *Comput. Mater. Sci.* **1996**, *6*, 15−50.
(58) Kresse, G.; Furthmuller, J. Efficient Iterative Schemes for *ab initio* Total-energy Calculations Using a Plane-wave Basis Set. *Phys. Rev. B: Condens. Matter Mater. Phys.* **1996**, *54* (16), 169−186.
(59) Perdew, J. P.; Burke, K.; Ernzerhof, M. Generalized Gradient Approximation Made Simple. *Phys. Rev. Lett.* **1996**, *77* (18), 3865−3868.


DOI: 10.1021/acsami.6b04375
*ACS Appl. Mater. Interfaces* 2016, 8, 18550−18559

(60) Kresse, G.; Joubert, D. From Ultrasoft Pseudopotentials to the Projector Augmented-wave Method. *Phys. Rev. B: Condens. Matter Mater. Phys.* **1999**, *59* (3), 1758−1775.
(61) Schmerler, S.; Kortus, J. Ab Initio Study of AlN: Anisotropic Thermal Expansion, Phase Diagram, and High-temperature Rocksalt to Wurtzite Phase Transition. *Phys. Rev. B: Condens. Matter Mater. Phys.* **2014**, *89* (6), 064109.
(62) Holec, D.; Mayrhofer, P. H. Surface Energies of AlN Allotropes from First Principles. *Scr. Mater.* **2012**, *67* (9), 760−762.
(63) Henkelman, G.; Arnaldsson, A.; Jónsson, H. A Fast and Robust Algorithm for Bader Decomposition of Charge Density. *Comput. Mater. Sci.* **2006**, *36* (3), 354−360.
(64) Sanville, E.; Kenny, S. D.; Smith, R.; Henkelman, G. Improved Grid-Based Algorithm for Bader Charge Allocation. *J. Comput. Chem.* **2007**, *28* (5), 899−908.
(65) Tang, W.; Sanville, E.; Henkelman, G. A Grid-Based Bader Analysis Algorithm Without Lattice Bias. *J. Phys.: Condens. Matter* **2009**, *21* (8), 1−7.
(66) Jonsson, H.; Mills, G.; Jacobsen, K. W. Nudged Elastic Band Method for Finding Minimum Energy Paths of Transitions. In *Classical and Quantum Dynamics in Condensed Phase Simulations*, Berne, B. J.; Ciccotti, G.; Coker, D. F., Eds.; World Scientific: Hackensack, NJ, 1998.
(67) Henkelman, G.; Uberuaga, B. P.; Jónsson, H. A Climbing Image Nudged Elastic Band Method for Finding Saddle Points and Minimum Energy Paths. *J. Chem. Phys.* **2000**, *113* (22), 9901−9904.
(68) Henkelman, G.; Jónsson, H. A Dimer Method for Finding Saddle Points on High Dimensional Potential Surfaces Using Only First Derivatives. *J. Chem. Phys.* **1999**, *111* (15), 7010−7022.
(69) Siegel, A.; Parlinski, K.; Wdowik, U. D. Ab Initio Calculation of Structural Phase Transitions in AlN Crystal. *Phys. Rev. B: Condens. Matter Mater. Phys.* **2006**, *74* (10), 104116.
(70) Madelung, O. *Semiconductors Data Handbook*; Springer-Verlag: Berlin, 2004; Vol. *8*.


DOI: 10.1021/acsami.6b04375
*ACS Appl. Mater. Interfaces* 2016, 8, 18550−18559